GREEN SYNTHESIS OF COPPER, ZINC, AND MAGNESIUM OXIDE NANOPARTICLES USING ORANGE PEEL EXTRACT

Denisa-Maria RADULESCU[1,3], Ionela Andreea NEACSU[1,2,3], Bodgan Stefan VASILE[2,3,4], Vasile-Adrian SURDU[1], Ecaterina ANDRONESCU[1,2, 3,*]

Over the years, nanoparticle development has been recognized as one of the most researched topics in materials science. Thus, their continuous assessment is strongly connected to their synthesis method and applicability in tissue engineering. Metal oxide nanoparticles have gained significant importance among various nanoparticles due to their outstanding antimicrobial properties. The improvement of their characteristics is highly influenced by the synthesis method. Considering this, the main concern about their route of fabrication through chemical methods is represented by the use of toxic solvents and precursors that lead to the generation of toxic by-products. Therefore, green synthesis by using bacteria, fungi, algae, and plant extracts or plant by-products is the most suitable alternative to overcome this drawback. This study aims to present the green synthesis of copper oxide, zinc oxide, and magnesium oxide nanoparticles (NPs), with average sizes of 10.48 nm (CuO), 9.08 nm (MgO), and 22.81 nm (ZnO), and their physicochemical characterization. The SEM images revealed a tendency to agglomerate, particularly in CuO and ZnO-based powders, with untreated ZnO NPs ranging from 100-190 nm and untreated CuO NPs exhibiting granular morphology with similar size characteristics. Post-calcination, CuO NPs' size reduced to 10-20 nm, ZnO NPs ranged from 3-15 nm, and MgO NPs were between 10-40 nm.

Keywords: green synthesis, nanoparticles, copper oxide, zinc oxide, magnesium oxide, properties, orange peel

1. Introduction

In recent years, the focus on nanotechnology has exponentially increased, especially for the research community. In this regard, nanotechnology allows the development of particles with tailored dimensions, less than 100 nm, which are further applied in numerous domains, such as biomedicine, energy, food industry, environment, and many others [1,2,3]. Hence, due to their small dimensions,

[1]* Department of Science and Engineering of Oxide Materials and Nanomaterials, Faculty of Chemical Engineering and Biotechnologies, National University of Science and Technology POLITEHNICA Bucharest, Romania, corresponding author, e-mail: ecaterina.andronescu@upb.ro

[2] Romanian Academy of Scientists, Bucharest, Romania

[3] National Research Center for Micro and Nanomaterials, Faculty of Chemical Engineering and Biotechnologies, National University of Science and Technology POLITEHNICA Bucharest, Romania

[4] Research Center for Advanced Materials, Products and Processes, National University of Science and Technology POLITEHNICA Bucharest, Romania

nanoparticles (NPs) are considered materials that exhibit improved properties (morphology, particle distribution, and excellent surface-to-volume ratio) compared with bulk materials [4]. Additionally, NPs can be synthesized in various shapes by using different routes, such as chemical, physical, or biological methods [5].

Furthermore, the development and research of metallic NPs have been amplified, particularly in the tissue engineering field, due to their increased antibacterial and antifungal properties. These nanomaterials include silver (Ag), gold (Au), and copper (Cu) NPs, which exhibit superior antimicrobial activity against various pathogens [6]. On the other hand, metal oxide NPs, such as titanium oxide (TiO_2), zinc oxide (ZnO), and copper oxide (CuO), are also widely studied for their outstanding stability and biocompatibility. These materials offer many advantages, such as high stability, simple preparation processes, ease of manufacturing in the desired shape, porosity, size, and facile incorporation into hydrophobic and hydrophilic systems. The synthesis of these oxides is an essential research topic, particularly due to their biomedical applications [7,8].

Another important characteristic of metal NPs incorporation is represented by the high control over the features of scaffolds, such as optimizing their mechanical strength and offering the controlled release of bioactive agents [9,10]. Even if many studies concluded that metal NPs exhibited toxicity, recent research demonstrated that the proper dosage, size, and size distribution reduce the toxicity of the developed materials. Due to their nature and ease of functionalization, the main properties of these materials could lead to an improved therapeutic effect [11]. In addition, the use of metal oxide NPs in tissue engineering can offer many advantages because of their outstanding properties such as high stability, simple preparation process, ease of manufacturing in the desired shape, porosity, size, and facile incorporation into hydrophobic and hydrophilic systems [12]. Nowadays, the main concerns about the synthesis method of metal oxide NPs are represented by their environmental impact. The most used synthesis routes are chemical or physical strategies [13,14]. The mentioned pathways use toxic agents that could produce potential hazards or exert carcinogenicity or environmental toxicity. These effects could be caused mainly by using harmful substances such as organic solvents, reducing agents, or stabilizers. Furthermore, using these toxic solvents limits the application of the developed nanomaterials in numerous biomedical or clinical applications. Hence, an eco-friendlier, clean, and reliable approach is needed [15,16].

To counter these limitations, green synthesis pathways have attracted significant attention in the research field. The use of green synthesis is currently preferred due to its capacity to reduce derivatives/pollution, prevention/minimization of waste, and the use of non-toxic (safer) solvents. In this regard, the most used natural sources are plants, fungi, bacteria, and algae [17].

Among the available methods of metal oxide NPs synthesis, the use of plant extracts and plant-derived materials is the most researched one from green synthesis routes, with an easy and simple fabrication process, offering the capacity to be reproduced on larger scales [18,19]. In this regard, the green pathway of NP formation not only uses plant-based materials as reducing agents for metal salts, but they also cover the synthesized NPs or even act as *in situ* capping and reducing agents. Their involvement in the formation process reduces toxicity, prevents nanoparticle agglomeration, and improves the antimicrobial activity of the nanomaterial, leading to a possible synergistic effect [20].

One of the most researched metal oxide NPs is the copper oxide (CuO) ones, as they offer many biological activities such as biocompatibility, antimicrobial, antidiabetic, and antioxidant activity, suitable for wound healing applications. [21]. In the last years, many studies have shown the successful development of CuO NPs by using waste plant products such as orange and citrus peel. El-Moslamy *et al*. [22] presented the use of citrus peel as a reducing and capping agent, allowing a more controlled synthesis route with a well-defined shape and size. Besides CuO NPs, ZnO NPs are one of the most used NPs in the bio-engineering field as they exhibit increased antioxidant, antifungal, antibacterial, and wound healing abilities, among many others. Hence, Rai *et al*. [23] have explained the successful synthesis of ZnO NPs using bacteria, plants, algae, or even fungi. According to their study, the basic properties of ZnO NPs are not altered, and their biological properties will be further improved. Moreover, MgO NPs have also received increased attention from researchers as they provide unique properties such as high chemical stability under extreme conditions and increased biocompatibility. In this sense, Ammulu *et al*. [24] explained that the prolonged antibacterial properties of MgO NPs are provided by the high-temperature tolerant properties and low volatility of the NPs. Additionally, Rotti *et al*. [25] have successfully synthesized MgO NPs by using neem, papaya, and mango leaf extracts through a simple solution combustion method. On the other hand, most green synthesis studies do not focus on the use of orange peel as the primary organic source. In general, the use of orange juice is preferred. Also, few studies have demonstrated the production of NPs using the same green source or the difference between them from a morphological point of view. The main purpose of this research is to present the reaction pathway in the synthesis of ZnO, MgO, and CuO-based NPs, by using orange peel as a reducing and capping agent and their further physico-chemical characterization.

2. Materials and Methods

2.1. Materials

For the CuO, ZnO, and MgO-based NPs synthesis, copper nitrate hemi(pentahydrate) (purchased from Sigma-Aldrich, 98%), zinc nitrate hexahydrate (purchased from Sigma-Aldrich, 98%), and magnesium nitrate

hexahydrate (purchased from Honeywell, Fluka, 98%) has been used. For the orange peel extract, 2 kg of oranges have been purchased from the local market.

2.2 Methods

In order to obtain the orange extract, the oranges were washed and peeled. The peel was placed in an oven at a temperature of 40 ℃ for 4 h. The dry peel was further crushed in a mortar for 30 min. The obtained powder was introduced into distilled water and magnetically stirred for 60 min. Following, the mixture was placed in an ultrasound bath at 60 ℃ for 1 h. The bath has been used to optimize the extraction of bioactive compounds from orange peel. This method should enhance efficiency, accelerate the process, preserve heat-sensitive compounds, and ensure uniform extraction. After that, the mixture was filtered, and the resulting extract was kept in the refrigerator for later use. The green synthesis of CuO and ZnO NPs followed a similar procedure, with the only difference being the metal precursors used. Initially, the specific metallic salt - either copper or zinc salts, depending on the desired NP - was combined with the orange extract and mixed for 60 min. Subsequently, this mixture was subjected to ultrasonic treatment in a bath set at 60℃ for 1 h. After this sonication process, the resulting NPs were then dried in an oven maintained at 150℃, followed by heat treatment at 400 ℃ for ZnO NPs and 300 ℃ for CuO NPs. Regarding the synthesis of Mg-based NPs, 2 solutions were prepared simultaneously, an orange extract solution and one containing the metal salt. The orange extract solution has been added (dropwise) to the metallic salt solution, followed by adjusting the pH to 12 using NH_3. Once the mixture reached pH 12, the solution was kept stirring for 4 h, followed by filtration, drying at 150 ℃, and heat treatment at 400 ℃.

2.3 X-Ray Diffraction (XRD) Analysis

X-ray diffraction analysis was carried out using PANalytical Empyrean equipment operated at 45 kV and 40 mA in Bragg-Brentanno geometry that uses CuKα radiation (λ=1.5418 Å). The diffractometer was equipped with a 0.02° Soller slit, 1/4° fixed divergent slit, and 1/2° anti-scatter slit on the incident beam side and a 0.02 mm Ni filter mounted on the PIXCel3D detector on the diffracted beam side. The parameters selected during measurement are a scan range of 10.0000 - 80.0107° 2θ, step size of 0.0263°, and counting time/step of 255s. Data reduction, search, and match procedures were performed using 3.0.e HighScorePlus software and the ICDD PDF4+ 2023 database.

2.5 Scanning Electron Microscopy (SEM) Analysis

Scanning Electron Microscopy was performed to determine the size and morphology of the green synthesized NPs. The images were recorded by using a Quanta Inspect F50 (FEI Company, Eindhoven, Netherlands) scanning electron microscope equipped with field emission gun electron (FEG).

3. Results and Discussion

3.1 X-Ray Diffraction (XRD)

The composition of the crystalline phases of the obtained powders was analyzed by X-ray diffraction, with the results presented in Fig. 1, 2, and 3. Fig. 1 shows the successful synthesis of CuO NPs using orange peel as a green synthesis route. The untreated Cu-based powder (Fig. 1) exhibited a single-phase composition of $Cu_2(OH)_3NO_3$ (PDF4+ 96-901-2716) with orthorhombic symmetry, identified by specific peaks at 2θ = 12°, 22°, 25°, 32°, 34°, 40°, 53°, 58°, and 62°, corresponding to the Miller indices (002), (111), (112), (201), (121), (213), (216), (321), and (234), respectively. After heat treatment at 300 ºC, the CuO powder showed successful formation of CuO NPs, as indicated by the PDF4+ 96-901-4581 file. These NPs exhibited monoclinic symmetry with specific peaks at 2θ = 32°, 35°, 38°, 48°, 58°, 61°, and 66°, corresponding to the Miller indices (110), (11-1), (111), (20-2), (202), (11-3), and (310), respectively, with an average crystallite size of 10.48 nm, value calculated by using the Debye-Scherrer equation [26].

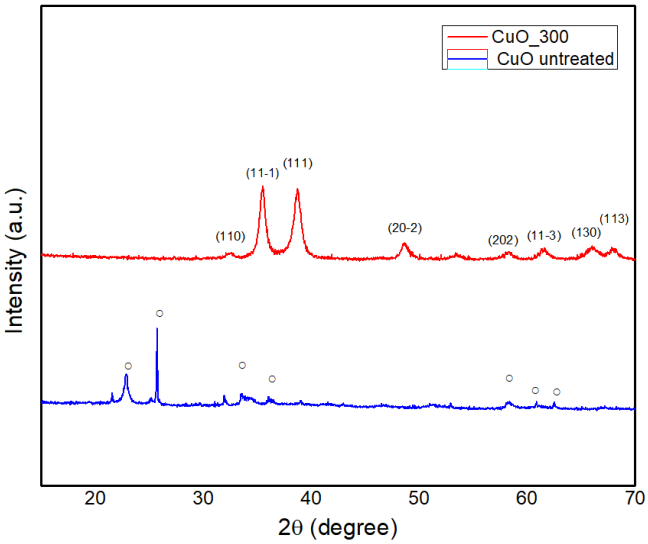

Fig. 1 X-ray diffractogram of green synthesized CuO NPs diffractogram where ○ - $Cu_2(OH)_3NO_3$

Fig. 2 demonstrates the hexagonal crystalline structure of untreated $Mg(OH)_2$ powder, referenced by database file number 96-210-1439. The specific peaks were observed around 2θ = 18°, 32°, 38°, 50°, and 58°, corresponding to the Miller indices (001), (100), (011), (012), and (110). Upon heat treatment at 400 ºC, the MgO powder formed MgO NPs, corresponding to the PDF4+ 04-016-2776 file, with cubic symmetry. The specific peaks were located at 2θ = 42°, 62°, 74°, and 78°, corresponding to the Miller indices (200), (220), (311), and (222), respectively, with an average crystallite size of 9.08 nm.

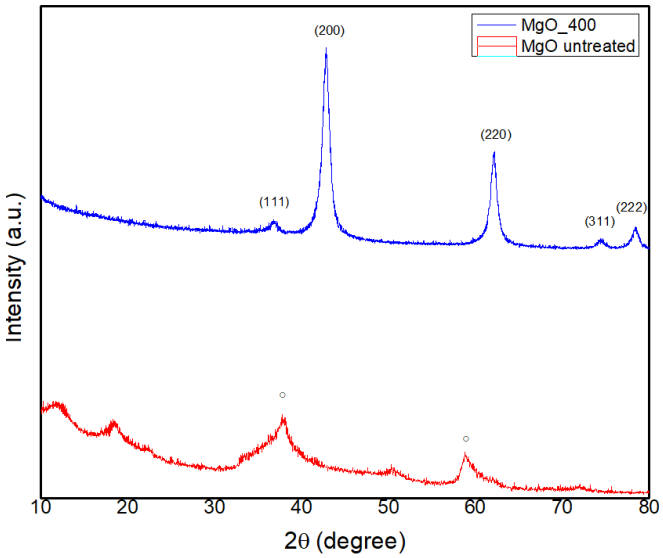

Fig. 2 X-ray diffractogram of green synthesized MgO NPs diffractogram where ○ - $Mg(OH)_2$

In the case of the untreated ZnO-based powder (Fig. 3), the synthesis resulted in a two-phase composition: $Zn_3(NO_3)_2(OH)_4$ (ICDD PDF4+ 04-014-0671) and $Zn(NO_3)_2 \cdot 2Zn(OH)_2$ (ICDD PDF4+ 00-018-1486).

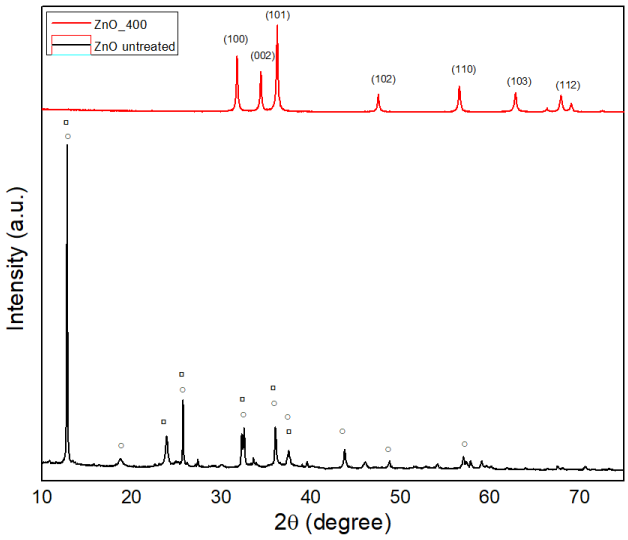

Fig. 3 X-ray diffractogram of green synthesized ZnO NPs diffractogram ○ - $Zn_3(NO_3)_2(OH)_4$ and ▫ - $Zn(NO_3)_2 \cdot 2Zn(OH)_2$

Upon curing at 400ºC, ZnO NPs were successfully obtained, corresponding to the PDF4+ 01-090-0391 file, with hexagonal symmetry. The specific peaks were observed at 2θ = 31°, 34°, 36°, 47°, 56°, 63°, and 67°, corresponding to the Miller

indices (100), (002), (101), (102), (110), (103), and (112), respectively, with an average crystallite size of 22.81 nm.

In conclusion, the heat treatment for all NPs leads to the formation of metal oxide NPs. This process involved the removal of volatile components (e.g., water, NOx) and the reorganization of remaining atoms into a stable oxide structure. The crystalline symmetry can change with the formation of the oxide phase, as observed with CuO (orthorhombic to monoclinic) and MgO (hexagonal to cubic). These phenomena are crucial for tailoring the properties of NPs for specific applications, as the crystalline structure and size significantly influence their physical and chemical behavior.

3.3 Scanning Electron Microscopy (SEM)

The SEM micrographs illustrate the morphology of the NPs obtained after synthesis, both before and after calcination. As shown in Fig. 4, all untreated NPs tend to agglomerate. This tendency is more pronounced in the CuO and ZnO-based powders compared to the Mg-based powder. At lower magnifications, the particles synthesized via the same green route display an irregular arrangement with significant interparticle spaces. For the untreated MgO-based NPs (Fig. 4e), the agglomeration of fine particles is less severe compared to the untreated CuO and ZnO-based NPs, which exhibit a more dispersive arrangement. The primary cause of agglomeration in these materials is likely due to the presence of organic residues from the orange extract used in the synthesis. These organic compounds can act as binders, causing particles to stick together and form larger aggregates. The SEM images of untreated ZnO-based NPs (Fig.4 c) show agglomerates with sizes ranging from 100 to 190 nm, exhibiting a polyhedral morphology. In contrast, the untreated CuO-based NPs (Fig. 4a) display a granular morphology with similar size characteristics to the ZnO-based powders. The untreated MgO-based NPs, however, have a smaller dimension, ranging from 10 to 30 nm, and exhibit a needle-like morphology.

After calcination, the agglomeration tendency diminishes, and the particle size of all CuO, ZnO, and MgO NPs decreases, resulting in smaller nanoparticles than those in the untreated samples. This reduction in agglomeration and particle size can be attributed to the removal of organic residues and the enhanced atomic mobility at elevated temperatures, which promotes better crystallite alignment and growth into smaller, more stable particles. Specifically, the size of CuO NPs (Fig. 4b) decreases to 10-20 nm, with a reduced tendency to agglomerate. The ZnO nanoparticles (Fig. 4d) also show a decrease in size, ranging from 3 to 15 nm, with a reduced agglomeration tendency compared to the untreated samples.

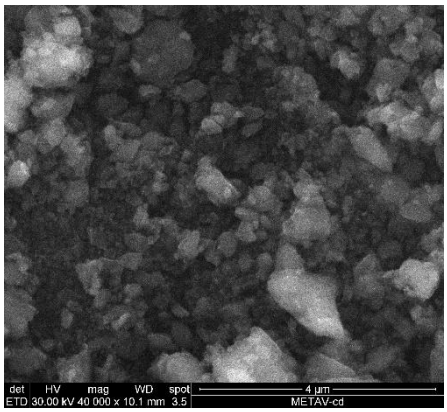

(a) CuO untreated x40,000 magnification

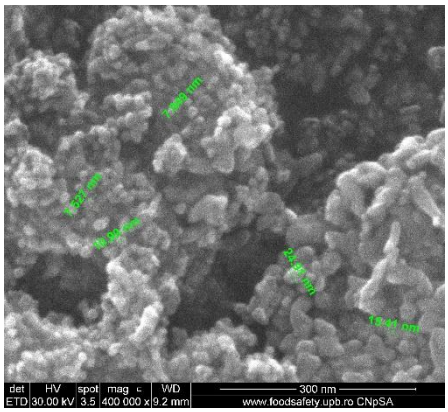

(b) CuO_300 – x400,000

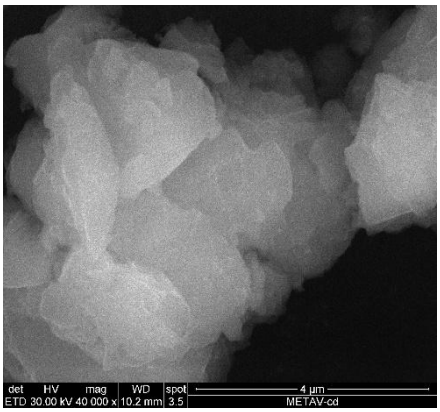

(c) ZnO untreated x40,000 magnification

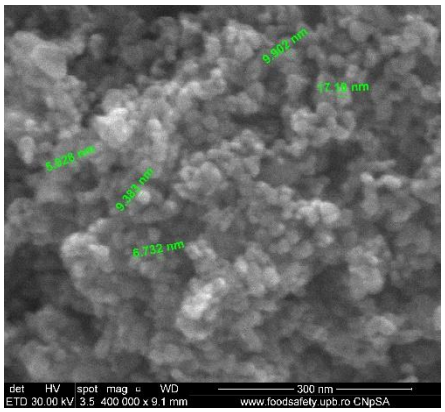

(d) ZnO_400 – x400,000

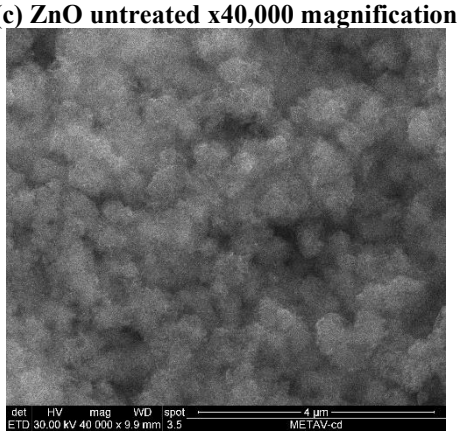

(e) MgO untreated - x40,000 magnification

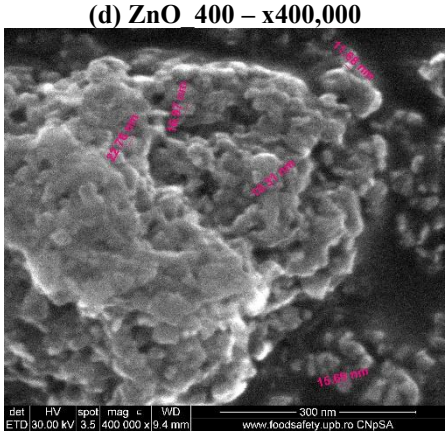

(f) MgO_400 x400,000

Fig. 4 SEM images of CuO, ZnO, and MgO NPs.

However, they still agglomerate more than CuO NPs due to their smaller size and high surface energy, which makes them more prone to form soft agglomerates. In the case of MgO NPs (Fig. 4f), the agglomeration tendency is

higher than in the other calcinated samples but less than in the untreated MgO NPs, while the particle size ranges between 10-40 nm. This indicates that while calcination reduces agglomeration, MgO NPs still tend to cluster compared to their CuO and ZnO counterparts. This agglomeration can be attributed to the inherent properties of MgO, such as its specific surface energy and the presence of any remaining surface hydroxyl groups that may facilitate particle interactions. In addition, the histogram in Fig. 5 indicates that the mean size of CuO nanoparticles is about 13.54 ± 1.421 nm, while ZnO nanoparticles have an average size of 17.01 ± 1.24 nm. This suggests a relatively uniform size distribution for both nanoparticle types, with only minor variations indicated by the standard deviation. Related to the MgO NPs, the mean size of the NPs is about 12.97 ± 1.24 nm.

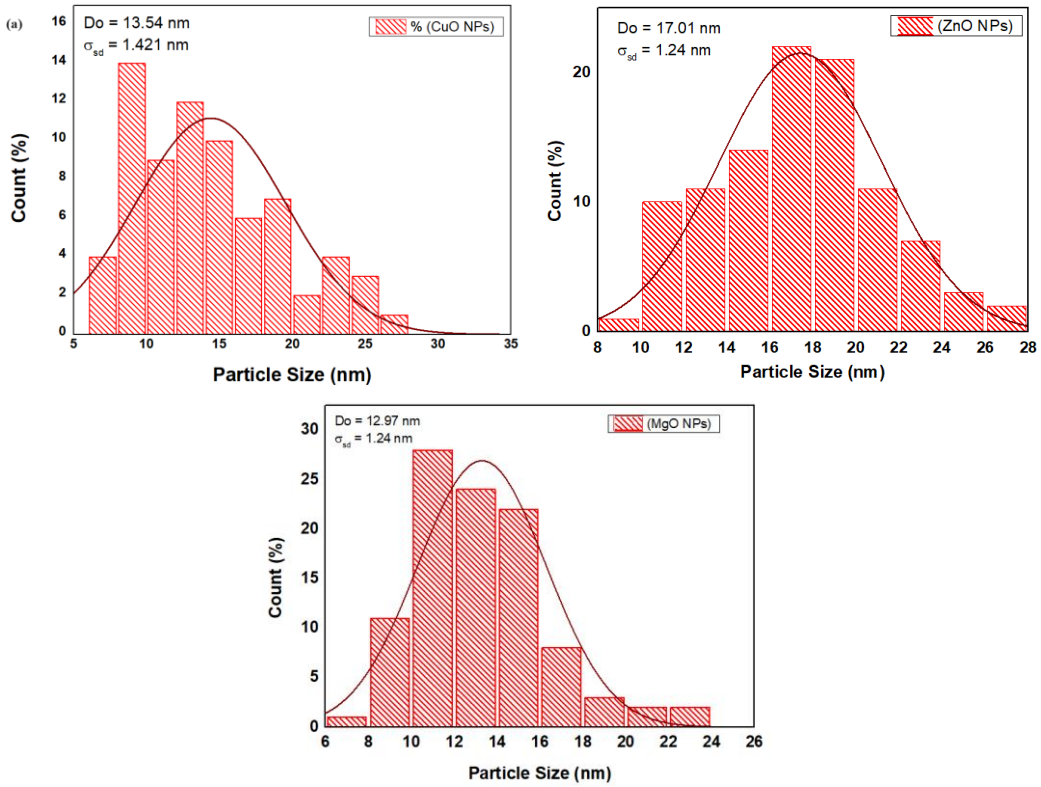

Fig. 5. Distributions and the average size of (a) CuO, (b) ZnO and (c) MgO NPs

The comparison between the particle sizes observed in SEM and the crystallite sizes calculated from XRD reveals important insights about the crystallinity of CuO, MgO, and ZnO nanoparticles (NPs). For CuO NPs, the SEM sizes (10-20 nm, with an average of 13.54 ± 1.421 nm) are closely aligned with the XRD crystallite size (10.48 nm), suggesting that these particles are monocrystalline, where each particle is a single crystallite. In the case of MgO NPs, the SEM sizes

(10-40 nm, with an average of 12.97 ± 1.24 nm) are slightly larger but still comparable to the XRD size (9.08 nm), indicating that these particles are likely monocrystalline or contain a small number of crystallites per particle. However, for ZnO NPs, the SEM sizes (3-15 nm, with an average of 17.01 ± 1.24 nm) are significantly smaller than the XRD crystallite size (22.81 nm), suggesting a polycrystalline nature, where each particle consists of multiple smaller crystallites. Therefore, the degree of similarity between SEM and XRD analysis confirms if the NPs are monocrystalline or polycrystalline, with CuO and MgO NPs leaning towards monocrystallinity and ZnO NPs being polycrystalline. [27].

4. Conclusions

In this study, CuO, ZnO, and MgO NP's were successfully synthesized using green synthesis methods with orange peel extract. The biomolecules from the orange peel extract acted as reducing agents, providing electrons to the metal ions and reducing them to their elemental states. These atoms served as nucleation centers, facilitating the growth of larger NPs through the combination of smaller particles. The ability of the orange peel extract to stabilize the NP's ultimately determined their energetically stable morphology. The X-ray diffraction (XRD) analysis confirmed the successful formation of CuO, MgO, and ZnO NPs post-calcination, with distinct crystalline phases observed for each type of NP. CuO NP's transitioned from orthorhombic $Cu_2(OH)_3NO_3$ to monoclinic CuO, MgO NPs transitioned from hexagonal $Mg(OH)_2$ to cubic MgO, and ZnO NPs transitioned from a mixture of $Zn_3(NO_3)_2(OH)_4$ and $Zn(NO_3)_2{\cdot}2Zn(OH)_2$ to hexagonal ZnO. The calcination process resulted in the decomposition of hydroxide and nitrate groups, forming stable oxide structures.

Scanning electron microscopy (SEM) revealed that untreated NP's exhibited a tendency to agglomerate, particularly in the case of CuO and ZnO-based powders. The agglomeration was attributed to organic residues from the orange peel extract. However, calcination minimized the agglomeration and reduced the particle sizes. CuO NPs reduced to 10-20 nm with minimal agglomeration, ZnO NPs reduced to 3-15 nm, and MgO NP's displayed a needle-like morphology with a higher tendency to cluster than the calcinated CuO and ZnO NP's. These findings underscore the effectiveness of orange peel extract in the green synthesis of metal-based NP's, demonstrating its potential as a sustainable and eco-friendly reducing and stabilizing agent. Further research is recommended to explore the physicochemical and biological properties of these NP's, particularly after calcination, to evaluate their applicability in various fields.

REFERENCES

[1] *G. Pal, P. Rai, A. Pandey.* Chapter 1 - Green synthesis of nanoparticles: A greener approach for a cleaner future, Micro and Nano Technologies, Green Synthesis, Characterization and Applications of Nanoparticles, Elsevier, Amsterdam, Netherlands, 2019, 1-26.

[2] *M. Huston, M. DeBella, M. DiBella, A. Gupta,* A. Green Synthesis of Nanomaterials, Nanomaterials 2021, **vol. 11**, no. 8, 2130.

[3] *A. Gour, N.K. Jain,* Advances in green synthesis of nanoparticles, Artificial Cells, Nanomedicine, and Biotechnology, 2019, **vol. 47**, no. 1, 844-851.

[4] *S.M. Rakib-Uz-Zaman, E. Hoque Apu, M.N. Muntasir, S.A. Mowna, M.G. Khanom, S.S. Jahan, N. Akter, M.A. R. Khan, N.S. Shuborna, S.M. Shams, K. Khan,* Biosynthesis of Silver Nanoparticles from Cymbopogon citratus Leaf Extract and Evaluation of Their Antimicrobial Properties, Challenges, 2022, **vol. 13,** no. 1, 18.

[5] *S., Kaabipour, S. Hemmati,* A review on the green and sustainable synthesis of silver nanoparticles and one-dimensional silver nanostructures, Beilstein J. Nanotechnol., 2021, **vol. 12**, 102–136.

[6] *D. MubarakAli, N. Thajuddin, K. Jeganathan, M. Gunasekaran,* Plant extract mediated synthesis of silver and gold nanoparticles and its antibacterial activity against clinically isolated pathogens, Colloids and Surfaces B: Biointerfaces, 2011, vol. 85, no. 2, 360-365.

[7] *O. Erdogan, M. Abbak, G.M. Demirbolat, F. Birtekocak, M. Aksel, S. Pasa, O. Cevik,* Green synthesis of silver nanoparticles via *Cynara scolymus* leaf extracts: The characterization, anticancer potential with photodynamic therapy in MCF7 cells, PLOS ONE, 2019, **vol.14,** no. 6, e0216496.

[8] *P.K. Tyagi, C. Quispe, J. Herrera-Bravo, S. Tyagi, D.B. Mrunal, M. Kumar, A.S. Dablool, S. Alghamdi, G. El-Saber Batiha, J. Sharifi-Rad, S. Ramniwas,* Synthesis of Silver and Gold Nanoparticles: Chemical and Green Synthesis Method and Its Toxicity Evaluation against Pathogenic Bacteria Using the ToxTrak Test, Journal of Nanomaterials,2021, **vol. 2021**, 3773943.

[9] M. Fathi-Achachelouei, H. Knopf-Marques, C.E. Ribeiro da Silva, J. Barthès, E. Bat, A. Tezcaner, N.E. Vrana, Use of Nanoparticles in Tissue Engineering and Regenerative Medicine, Front. Bioeng. Biotechnol., 2019, vol. 7, 113.

[10] *D.-M. Radulescu, I.A. Neacsu, A.-M. Grumezescu, E. Andronescu*, New Insights of Scaffolds Based on Hydrogels in Tissue Engineering, *Polymers*, 2022; vol. 14, no. 4, 799.

[11] *R. Eivazzadeh-Keihan, E. Bahojb Noruzi, K. Khanmohammadi Chenab, A. Jafari, F. Radinekiyan, S.M. Hashemi, F. Ahmadpour, A. Behboudi, J. Mosafer, A. Mokhtarzadeh, A. Maleki, M.R. Hamblin,* Metal-based nanoparticles for bone tissue engineering, J Tissue Eng Regen Med, 2020, vol. 14, 1687–1714.

[12] *R. Gobi, P. Ravichandiran, R.S. Babu, D.J. Yoo.* Biopolymer and Synthetic Polymer-Based Nanocomposites in Wound Dressing Applications: A *Review,* Polymers, 2021, **vol. 13,** no. 12, 1962.

[13] *M. Aravind, M. Amalanathan, M.S.M. Mary,* Synthesis of TiO2 nanoparticles by chemical and green synthesis methods and their multifaceted properties, SN Applied Sciences, 2021, **vol. 3,** no. 409, 1-10.

[14] *H.C.A. Murthy, B. Abebe, C.H. Prakash, K. Shantaveerayya,* A Review on Green Synthesis of Cu and Cuo Nanomaterials for Multifunctional Applications, Mat.Sci.Res.India, 2018, **vol. 15**, no. 3.

[15] *D. Zhang*, *X.-L. Ma*, *Y. Gu*, *H. Huang*, *G.-W. Zhang*, Green Synthesis of Metallic Nanoparticles and Their Potential Applications to Treat Cancer, Front. Chem, 2020, **vol. 8**, 799.

[16] *S. Ying, Z. Guan, P.C. Ofoegbu, P. Clubb, C. Rico, F. He, J. Hong,* Green synthesis of nanoparticles: Current developments and limitations, Environmental Technology & Innovation, 2022, **vol. 26**, 102336.

[17] *P. Kaushal, N. Verma, K. Kaur, A.K. Sidhu,* Green Synthesis: An Eco-friendly Route for the Synthesis of Iron Oxide Nanoparticles, Front. Nanotechnol., 2021, vol. 3, 655062.

[18] *J. Singh, T. Dutta, K.H. Kim, M. Rawat, P. Samddar, P. Kumar*, 'Green' synthesis of metals and their oxide nanoparticles: applications for environmental remediation, J Nanobiotechnol, 2018, **vol. 16,** 84.

[19] *H. Jahangirian, E.G. Lemraski, R. Rafiee-Moghaddam, T.J. Webster*, A review of using green chemistry methods for biomaterials in tissue engineering. International journal of nanomedicine, 2018, **vol. 13,** 5953–5969.

[20] *A. Roy, O. Bulut, S. Some, A.K. Mandal, M.D. Yilmaz,* Green synthesis of silver nanoparticles: Biomolecule-nanoparticle organizations targeting antimicrobial activity, RSC Adv., 2019, **vol. 9**, no. 5, 2673–2702.

[21] *S. Ghosh, T.J. Webster*, Metallic Nanoscaffolds as Osteogenic Promoters: Advances, Challenges and Scope, Metals, 2021, **vol. 11**, no. 9, 1356

[22] *S.H. El-Moslamy, H.S. Hassan, A.H. Rezk, Y,R. Abdel-Fattah*, Bioprocess Strategies and Characterization of Anti- Multidrug Resistant Human Pathogens Copper/Copper Oxide Nanoparticles from Citrus Peel Waste Extracts, Journal of Nanomaterials & Molecular Nanotechnology, 2017, **vol. 6**, 1-14.

[23] *R.S. Rai, J. P. Girish, V. Bajpai, M.I. Khan, N. Elboughdiri, A. Shanableh, R. Luque*, An eco-friendly approach on green synthesis, bio-engineering applications, and future outlook of ZnO nanomaterial: A critical review, Environmental Research, 2023, **vol. 221**, 114807.

[24] *M.A. Ammulu, V.K. Vinay, K. A.K. Giduturi, P.K. Vemuri, U. Mangamuri, S. Poda*, Phytoassisted synthesis of magnesium oxide nanoparticles from Pterocarpus marsupium rox.b heartwood extract and its biomedical applications. J Genet Eng Biotechnol, 2021, **vol. 19**, 21.

[25] *R.B. Rotti, D.V. Sunitha, R. Manjunath, A. Roy, S.B. Mayegowda, A.P. Gnanaprakash, S. Alghamdi, M. Almehmadi, O. Abdulaziz, M. Allahyani, A. Aljuaid, A.A. Alsaiari, S.S. Ashgar, A.O. Babalghith, A.E. Abd El-Lateef, E.B. Khidir*, Green synthesis of MgO nanoparticles and its antibacterial properties. Front. Chem., 2023, **vol. 11**, 1143614.

[26] *M. Zakirov, M.P. Semen'ko, O.A. Korotchenkov*. A Simple Sonochemical Synthesis of Nanosized ZnO from Zinc Acetate and Sodium Hydroxide. J. Nano- Electron. Phys., 2018, **vol. 10**, 05023.

[27] *Q. Li, C.W. Kartikowati, S. Horie, T. Oji, T. Iwaki, K. Okuyama*. Correlation between particle size/domain structure and magnetic properties of highly crystalline Fe_3O_4 nanoparticles. Sci. Rep. 2017, **vol. 7**, 9894.